

MHD α^2 -dynamo, Squire equation and \mathcal{PT} -symmetric interpolation between square well and harmonic oscillator

Uwe Günther^{a)} and Frank Stefani^{b)}

Research Center Rossendorf, P.O. Box 510119, D-01314 Dresden, Germany

Miloslav Znojil^{c)}

Ústav Jaderné Fyziky AV ČR, 250 68 Řež, Czech Republic

(Received 28 January 2005; accepted 18 March 2005; published online 17 May 2005)

It is shown that the α^2 -dynamo of magnetohydrodynamics, the hydrodynamic Squire equation as well as an interpolation model of \mathcal{PT} -symmetric quantum mechanics are closely related as spectral problems in Krein spaces. For the α^2 -dynamo and the \mathcal{PT} -symmetric model the strong similarities are demonstrated with the help of a 2×2 operator matrix representation, whereas the Squire equation is reinterpreted as a rescaled and Wick-rotated \mathcal{PT} -symmetric problem. Based on recent results on the Squire equation the spectrum of the \mathcal{PT} -symmetric interpolation model is analyzed in detail and the Herbst limit is described as spectral singularity. © 2005 American Institute of Physics. [DOI: 10.1063/1.1915293]

I. INTRODUCTION

Non-Hermitian \mathcal{PT} -symmetric quantum mechanical systems^{1–8} are known to possess spectral sectors with purely real eigenvalues as well as sectors with pairs of complex conjugate eigenvalues. Changes of certain system parameters can lead to spectral phase transitions from one sector to the other. The physics in the two sectors has been identified with phases of unbroken \mathcal{PT} -symmetry (real eigenvalues) and spontaneously broken \mathcal{PT} -symmetry (pairwise complex conjugate eigenvalues).^{1,2} From a mathematical point of view, non-Hermitian \mathcal{PT} -symmetric Hamiltonians are self-adjoint operators in Krein spaces^{9–11}—Hilbert spaces with an additional indefinite metric structure—and the two spectral sectors correspond to Krein space states of positive or negative type (real eigenvalues) and neutral (isotropic) states (pairwise complex conjugate eigenvalues).

Apart from \mathcal{PT} -symmetric quantum mechanics (PTSQM), it is known that a certain class of spherically symmetric mean-field dynamo models¹² of magnetohydrodynamics (MHD) can be described by self-adjoint operators in Krein spaces as well.¹³ These models show similar spectral phase transitions from real to pairwise complex conjugate eigenvalues¹⁴—and only the physical interpretation differs from that in PTSQM. For dynamos it simply consists in a transition from nonoscillatory states to oscillatory states.

In the present paper, we are going to briefly describe the underlying structural operator theoretic parallels between PTSQM models and the spherically symmetric MHD α^2 -dynamo (Sec. II). The discussion will be illustrated with the help of a \mathcal{PT} -symmetric interpolation between a harmonic oscillator placed in a square well and an empty square well (Sec. III). This interpolation shows a rich structure of spectral phase transitions with a couple of unexpected features. Furthermore, we will show in Sec. IV that the eigenvalue problem of the \mathcal{PT} -symmetric (intermediate) interpolation model with linear complex potential (purely complex electrical field) within the square well is mathematically identical to the eigenvalue problem of the rescaled and Wick-rotated

^{a)}Electronic mail: u.guenther@fz-rossendorf.de

^{b)}Electronic mail: f.stefani@fz-rossendorf.de

^{c)}Electronic mail: znojil@ujf.cas.cz

Squire equation of hydrodynamics which describes the normal vorticity of a plane channel flow (Couette flow) with linear transversal velocity profile. Recent Airy function based results on the Squire equation allow us to analytically describe the spectral behavior of the PTSQM model in the limiting case when the width of the square well tends to infinity. In this limit we reproduce the Herbst model¹⁵ with its empty spectrum. The limiting behavior occurs as a blowing-up of the spectrum to infinity along three directions on the complex plane—leaving behind a spectrally empty region at any fixed finite distance from the origin of the spectral plane. In Sec. V we briefly sketch some links of the obtained results to other physical setups and analytical techniques.

II. KREIN SPACE PROPERTIES OF \mathcal{PT} -SYMMETRIC QUANTUM MODELS AND OF THE SPHERICALLY SYMMETRIC MHD α^2 -DYNAMO

A. \mathcal{PT} -symmetric quantum models

In their seminal letter¹ Bender and Boettcher identified \mathcal{PT} -symmetry as the essential property of the non-Hermitian quantum system,

$$H\psi(x) = E\psi(x), \quad H = -\frac{d^2}{dx^2} + gx^2(ix)^\nu, \quad (1)$$

which ensures the reality of its spectrum for exponents $\nu \in [0, 2)$ and $\psi(x) \in \tilde{\mathcal{H}} = L_2(-\infty, \infty)$.¹⁶ This allowed them not only to extend an earlier conjecture of Bessis and Zinn-Justin [whose numerical results indicated that quantum systems with complex potential $V(x) = ix^3$ might have a purely real spectrum], but also initiated the still lasting intensive study of generalized \mathcal{PT} -symmetric non-Hermitian systems.¹⁷ Such systems are characterized by a \mathcal{PT} -symmetric Hamiltonian H ,

$$[\mathcal{PT}, H] = 0, \quad (2)$$

where \mathcal{P} denotes a reflection

$$\mathcal{P}x\mathcal{P} = -x, \quad \mathcal{P}\psi(x) = \psi(-x),$$

while the time-reversal operator \mathcal{T} performs complex conjugation,

$$\mathcal{T}i\mathcal{T} = -i, \quad \mathcal{T}\psi(x) = \psi(x)^*. \quad (3)$$

Because both operators \mathcal{P} and \mathcal{T} are involution operators,

$$\mathcal{P}^2 = I, \quad \mathcal{T}^2 = I,$$

they induce natural \mathbb{Z}_2 -gradings of the Hilbert space $\tilde{\mathcal{H}}$. For our subsequent analysis it suffices to consider the subclass of models which can be defined solely over the real line $x \in \mathbb{R}$. For such models the \mathcal{T} -induced \mathbb{Z}_2 -grading corresponds to a splitting of the wave functions $\psi \in \tilde{\mathcal{H}}$ into real and imaginary components (what is of no direct physical interest in a quantum mechanical context; additionally one would have to work in a real Hilbert space with doubled dimension compared to the original complex one), whereas \mathcal{P} induces a \mathbb{Z}_2 -grading into parity even and parity odd components,

$$\psi(x) = \psi_+(x) + \psi_-(x), \quad \mathcal{P}\psi_\pm(x) = \psi_\pm(-x) = \pm \psi_\pm(x). \quad (4)$$

The corresponding \mathbb{Z}_2 -graded Hilbert space splits as

$$\tilde{\mathcal{H}} = \mathcal{H}_+ \oplus \mathcal{H}_-, \quad \psi_\pm \in \mathcal{H}_\pm.$$

In the case of a simple \mathcal{PT} -symmetric one-particle system with Hamiltonian

$$H = -\partial_x^2 + V_+(x) + iV_-(x), \quad V_\pm(-x) = \pm V_\pm(x), \quad \Im V_\pm = 0 \quad (5)$$

it holds

$$H = \mathcal{P}H^\dagger\mathcal{P} \quad (6)$$

and \mathcal{P} is a so called fundamental (canonical) operator symmetry^{9,10} of H —i.e., H is \mathcal{P} -pseudo-Hermitian in the sense of Refs. 4 and 5. Operators with an involutive fundamental symmetry are known to be symmetric—and for appropriately chosen domain [boundary conditions for the functions $\psi(x)$] even self-adjoint—in a Krein space \mathcal{K} . For \mathcal{P} -pseudo-Hermitian operators over the real line this Krein space $\mathcal{K}_\mathcal{P}$ is given as^{11,18,19}

$$(\mathcal{K}_\mathcal{P}, [\cdot, \cdot]_\mathcal{P}), \quad [\psi, \phi]_\mathcal{P} = (\psi, \mathcal{P}\phi) = \int_{C \subseteq \mathbb{R}} \psi^*(x)\mathcal{P}\phi(x)dx = \int_{C \subseteq \mathbb{R}} \psi^*(x)\phi(-x)dx. \quad (7)$$

Depending on the concrete problem, the integration in (7) is performed over a finite interval, $C = [-a, a]$, or over the complete real line, $C = (-\infty, \infty) \sim \mathbb{R}$. From (5) and (6) one immediately finds

$$[H\psi, \phi]_\mathcal{P} = [\psi, H\phi]_\mathcal{P}.$$

The Krein space inner (scalar) product $[\psi, \phi]_\mathcal{P}$ has the following properties:

- (i) It coincides with the more general \mathcal{PT} inner product of Bender *et al.*,^{6,7}

$$(\psi, \phi)_{\mathcal{PT}} = \int_{C \subset \mathbb{C}} [\mathcal{PT}\psi(x)]\phi(x)dx$$

when the integration path $C \subset \mathbb{C}$ of the latter integral is restricted to (an interval of) the real line, $C \subseteq \mathbb{R}$,

$$(\psi, \phi)_{\mathcal{PT}} = \int_{C \subseteq \mathbb{R}} [\mathcal{PT}\psi(x)]\phi(x)dx = \int_{C \subseteq \mathbb{R}} [\mathcal{P}\psi(x)^*]\phi(x)dx = \int_{C \subseteq \mathbb{R}} \psi(x)^*\mathcal{P}\phi(x)dx = [\psi, \phi]_\mathcal{P}.$$

- (ii) In contrast to the “usual” positive definite metric structure of the Hilbert space $\tilde{\mathcal{H}} = \mathcal{H}_+ \oplus \mathcal{H}_-$,

$$(\tilde{\mathcal{H}}, (\cdot, \cdot)), \quad (\psi, \phi) = \int_{C \subseteq \mathbb{R}} \psi^*(x)\phi(x)dx = \int_{C \subseteq \mathbb{R}} (\psi_+^*\phi_+ + \psi_-^*\phi_-)dx,$$

with non-negative norm

$$\|\psi\|^2 = (\psi, \psi) = \|\psi_+\|^2 + \|\psi_-\|^2 \geq 0,$$

the scalar product $[\psi, \phi]_\mathcal{P}$ defines an indefinite metric structure in the Krein space $\mathcal{K}_\mathcal{P} = \mathcal{H}_+ \oplus \mathcal{H}_-$, what is easily seen from the decomposition (4)

$$[\psi, \phi]_\mathcal{P} = \int_{C \subseteq \mathbb{R}} (\psi_+^*\phi_+ - \psi_-^*\phi_-)dx.$$

- (iii) In rough analogy with timelike, spacelike, and lightlike (isotropic) vectors in Minkowski space, one distinguishes Krein space vectors of positive type, $[\psi_+, \psi_+]_\mathcal{P} = \|\psi_+\|^2 > 0$, of negative type, $[\psi_-, \psi_-]_\mathcal{P} = -\|\psi_-\|^2 < 0$, and neutral (isotropic) vectors,

$$[\psi, \psi]_\mathcal{P} = 0, \quad \psi = \psi_+ + \psi_-, \quad \|\psi_+\|^2 = \|\psi_-\|^2.$$

In order to make the structural Krein space analogies of PTSQM models and MHD dynamo setups maximally transparent, we rewrite the eigenvalue problem, $H\psi = E\psi$, for the \mathcal{PT} -symmetric Hamiltonian (5) in an equivalent 2×2 matrix operator representation. Introducing the projection operators

$$P_{\pm} := \frac{1}{2}(I \pm \mathcal{P})$$

we decompose wave function ψ and Hamiltonian H (see, e.g., Ref. 9) as

$$\psi = P_+ \psi + P_- \psi = \psi_+ + \psi_-,$$

$$H = P_+ H P_+ + P_- H P_+ + P_+ H P_- + P_- H P_-.$$

In terms of the notation

$$H_{\pm\pm} := P_{\pm} H P_{\pm} = -\partial_x^2 + V_{\pm}(x), \quad H_{\pm\mp} := P_{\pm} H P_{\mp} = iV_{\mp}(x) \quad (8)$$

this gives

$$\begin{pmatrix} H_{++} & H_{+-} \\ H_{-+} & H_{--} \end{pmatrix} \begin{pmatrix} \psi_+ \\ \psi_- \end{pmatrix} = E \begin{pmatrix} \psi_+ \\ \psi_- \end{pmatrix}, \quad \mathcal{P} = \begin{pmatrix} I & 0 \\ 0 & -I \end{pmatrix}, \quad (9)$$

where

$$H_{\pm\pm} = H_{\pm\pm}^{\dagger}, \quad H_{+-} = -H_{-+}^{\dagger}. \quad (10)$$

If one replaces the matrix entries in (9) and (10) by appropriate constants one arrives at the schematic two-level model

$$H_H \begin{pmatrix} u \\ v \end{pmatrix} = E \begin{pmatrix} u \\ v \end{pmatrix}, \quad H_H = \begin{pmatrix} c+a & b \\ -b^* & c-a \end{pmatrix}, \quad a, c \in \mathbb{R}, \quad (11)$$

which may be read as an elementary exemplification of Heisenberg's linear-algebraic approach²⁰ to (\mathcal{PT} -symmetric) quantum mechanics and which was intensively studied in Refs. 6, 7, 18, and 21–23.

B. The spherically symmetric MHD α^2 -dynamo

The magnetic fields of planets, stars, and galaxies are maintained by homogeneous dynamo effects, which can be successfully described within magnetohydrodynamics (MHD). One of the simplest dynamos is the spherically symmetric mean-field α^2 -dynamo in its kinematic regime. This dynamo model is capable to play a similar paradigmatic role in MHD dynamo theory like the harmonic oscillator in quantum mechanics (QM). Its operator matrix has the form (see the Appendix for a few comments on the origin of this operator matrix and on the physics of α^2 -dynamos)¹³

$$\hat{H}_l[\alpha] = \begin{pmatrix} -Q[1] & \alpha \\ Q[\alpha] & -Q[1] \end{pmatrix} \quad (12)$$

and consists of formally self-adjoint blocks

$$Q[\alpha] := p\alpha p + \alpha \frac{l(l+1)}{r^2},$$

where $p = -i(\partial_r + 1/r)$ denotes the radial momentum operator. The operator $\hat{H}_l[\alpha]$ is defined over an interval $\Omega = [0, 1] \ni r$ and acts on two-component vectors ϕ which describe the coupled

l -modes of the poloidal and toroidal magnetic field components of a mean-field dynamo model with helical turbulence function (α -profile) $\alpha(r)$.

Although the dynamo model is not \mathcal{PT} -symmetric, its operator $\hat{H}_l[\alpha]$ shares a basic underlying symmetry with PTSQM Hamiltonians—a \mathbb{Z}_2 -graded pseudo-Hermiticity (J -pseudo-Hermiticity)^{5,14} which is induced by the fundamental (canonical) symmetry,

$$\hat{H}_l[\alpha] = J\hat{H}_l^\dagger[\alpha]J, \quad J = \begin{pmatrix} 0 & I \\ I & 0 \end{pmatrix}.$$

Similar to the reflection operator \mathcal{P} in (6), the operator J is unitary and involutive

$$J^\dagger = J^{-1}, \quad J^2 = I.$$

The boundary conditions on the vector function ϕ are set at $r=1$ (the rescaled surface radius of the star or planet whose fluid/plasma motion maintains the dynamo effect) and it is assumed that $\alpha(r>1) \equiv 0$. In the case of physically idealized boundary conditions at $r=1$ (see, e.g., Ref. 24), the domain $\mathcal{D}(\hat{H}_l[\alpha])$ of the operator $\hat{H}_l[\alpha]$ consists of functions ϕ such that

$$\mathcal{D}(\hat{H}_l[\alpha]) := \left\{ \phi = \begin{pmatrix} \phi_1 \\ \phi_2 \end{pmatrix} : \phi \in \tilde{\mathcal{H}} \equiv \mathcal{H} \oplus \mathcal{H}, \mathcal{H} = L_2(\Omega, r^2 dr), \Omega = [0, 1], \phi(1) = 0, r\phi(r)|_{r \rightarrow 0} \rightarrow 0 \right\},$$

and $\hat{H}_l[\alpha]$ is self-adjoint in a Krein space

$$(\mathcal{K}_{\mathcal{J}}, [\cdot, \cdot]_{\mathcal{J}}), \quad [\psi, \phi]_{\mathcal{J}} = \int_0^1 \psi^\dagger J \phi r^2 dr, \quad [\hat{H}_l \chi, \phi]_{\mathcal{J}} = [\chi, \hat{H}_l \phi]_{\mathcal{J}}.$$

It should be noted that for physically realistic boundary conditions

$$\hat{B}_l \phi|_{r=1} = 0, \quad \hat{B}_l = \text{diag}[\partial_r + (l+1)/r, 1] \quad (13)$$

there exists no appropriate Krein space which could make the operator $\hat{H}_l[\alpha]$ J -self-adjoint.

The structures of PTSQM models and the α^2 -dynamo can be compared most explicitly after passing from $\mathcal{K}_{\mathcal{J}}$ to an equivalent Krein space \mathcal{K}_{μ} with diagonal metric operator μ and redefined Hilbert spaces components, $L_2(\Omega, r^2 dr) \mapsto L_2(\Omega, dr)$. The diagonalization yields

$$J \mapsto \mu := \begin{pmatrix} I & 0 \\ 0 & -I \end{pmatrix} = S^{-1}JS, \quad S = \frac{1}{\sqrt{2}} \begin{pmatrix} I & -I \\ I & I \end{pmatrix}, \quad (14)$$

$$\hat{H}_l[\alpha] \mapsto \check{H}_l[\alpha] = S^{-1}\hat{H}_l[\alpha]S = \frac{1}{2} \begin{pmatrix} Q[\alpha-2] + \alpha & -Q[\alpha] + \alpha \\ Q[\alpha] - \alpha & Q[-\alpha-2] - \alpha \end{pmatrix}, \quad (15)$$

$$\phi \mapsto \check{\phi} = \begin{pmatrix} \phi_+ \\ \phi_- \end{pmatrix} = \frac{1}{\sqrt{2}} \begin{pmatrix} \phi_2 + \phi_1 \\ \phi_2 - \phi_1 \end{pmatrix}, \quad (16)$$

whereas the unitary mapping $U: L_2(\Omega, r^2 dr) \mapsto L_2(\Omega, dr)$ simplifies the structure of $Q[\alpha]$ and leads in (15) and (16) to the additional replacements

$$\phi_{1,2} \mapsto f_{1,2} := r\phi_{1,2}, \quad Q[\alpha] \mapsto q[\alpha] := rQ[\alpha]r^{-1} = -\partial_r \alpha(r) \partial_r + \alpha(r) \frac{l(l+1)}{r^2}. \quad (17)$$

By inspection of (8)–(10) and (14)–(17) we find that, in the chosen Krein space representations of the PTSQM model and the α^2 -dynamo, the block structures of the metrics (involution operators) \mathcal{P} and μ coincide, $\mathcal{P} = \mu$, but that the blocks of the \mathcal{PT} -symmetric Hamiltonian and the dynamo operator show significant structural differences [in a very rough analogy, the alpha profile $\alpha(r)$ has

some similarities to a position depending mass, as it was studied for QM models, e.g., in Ref. 25],

$$H_{\pm\pm} = -\partial_x^2 + V_{\pm}(x) \leftrightarrow -q[1] \pm \frac{q[\alpha] + \alpha}{2},$$

$$H_{\pm\mp} = iV_{\mp}(x) \leftrightarrow \mp \frac{q[\alpha] - \alpha}{2}.$$

It is clear that these differences in the differential expressions (as well as the different boundary conditions on the two-component eigenfunctions) will lead to different global behaviors of the corresponding operator spectra. Nevertheless, both types of systems share the same Krein-space induced features of level crossings, what will be briefly sketched in the next section.

C. Spectral phase transitions

Since the first PTSQM paper¹ of Bender and Boettcher it is known that \mathcal{PT} -symmetric Hamiltonians have a real spectrum when \mathcal{PT} -symmetry is an exact symmetry and not spontaneously broken (the corresponding eigenfunctions are invariant under a \mathcal{PT} -transformation), whereas spontaneously broken \mathcal{PT} -symmetry is connected with complex energies. [We recall that this follows from (2) and (3), the eigenvalue equation $H\psi = E\psi$ and its \mathcal{PT} -transformed, $H\mathcal{PT}\psi = E^*\mathcal{PT}\psi$. For real eigenvalues, $E = E^*$, it is natural to set $\psi = \mathcal{PT}\psi$, whereas $E \neq E^*$ necessarily implies $\psi \neq \mathcal{PT}\psi$.] A consistent PTSQM applicability and interpretation of the complex-energy states remains an open question up to now (cf., e.g., Ref. 26). For convenience, we shall call these states “unphysical” here.

The mathematically most interesting questions of PTSQM concern the transition between the physical and unphysical domains of their parameters. In the simple two-state model (11) it is easy to deduce that the quantized energies E are real (“physical”) for $|a| > |b|$ while they form complex-conjugate pairs in the “unphysical” regime where $|a| < |b|$.^{7,18} The boundary of its PTSQM applicability coincides with the double-cone hypersurface in parameter space where $|a| = |b|$. One easily verifies that whenever $|b|$ approaches $|a|$, the separate eigenenergies E_{\pm} as well as the corresponding two independent bound-state eigenvectors coalesce and coincide. On the critical hypersurface the remaining (geometrical) eigenvector becomes supplemented by a so called associated vector (algebraic eigenvector)¹⁴ and the Hamiltonian matrix H acquires a Jordan-block canonical structure.^{14,27} The latter cannot be diagonalized and it only gives the doubly degenerate and real single “exceptional-point” eigenvalue $E = E_{(\text{EP})} = c$ (cf., e.g., Ref. 28 for more details).

An exhaustive and consistent bound-state interpretation of the Schrödinger-type equation (1) is more difficult. For example, it requires the restriction of the range of exponents to a finite interval of $\nu \in (-1, 2)$ for $\psi(x) \in L_2(-\infty, \infty)$ as usual defined on the real line.¹ A rigorous proof of the reality of the energies turned out unexpectedly difficult.^{16,29} For larger exponents ν , the real line must be replaced by an appropriately deformed contour in the complex plane.^{1,2}

A systematic analytical study of phase transition points is still lacking for PTSQM models; the same concerns efficient mathematical tools for deriving their location in parameter space. Similar to the double-cone hypersurfaces for the simple matrix model (11), one expects more complicated (and more interesting) global phase-transition hypersurfaces in case of the Schrödinger-type systems. Knowing the location of these phase transition hypersurfaces, one would know the boundaries of the “physical” regions of exact \mathcal{PT} -symmetry.

For the α^2 -dynamo both types of eigenvalues—real ones as well as pairwise complex conjugate ones—have a clear physical meaning. They simply correspond to nonoscillatory and oscillatory dynamo states, respectively. But again it is of utmost interest to know the parameter configurations for which transitions between the two types of states (phases) occur. In the recent paper,³⁰ strong numerical indications were presented that magnetic field reversals (interchanges of North and South poles as they are evident from paleomagnetic data on the Earth magnetic field³¹) are induced by a special type of nonlinear dynamics in the vicinity of spectral phase transition points. [In the concrete case, the nonlinear transition mechanism between kinematic and saturated dy-

namo regime (a brief outline of the corresponding physics can be found in the Appendix) was simulated with the help of a so called α -quenching (see, e.g., Ref. 32) which simulates the nonlinear back-reaction of the induced magnetic fields on the α -profile $\alpha(r)$.]

The qualitative features of the real-to-complex phase transitions are essentially the same for PTSQM models and for the MHD α^2 -dynamo. They correspond to transitions from Krein space states of positive and negative type to pairwise neutral (isotropic) states^{11,14}—and a square-root branching of the spectral Riemann surface.^{33,34} Such transitions are a generic feature of Krein-space setups and they are new compared with setups in Hilbert spaces with purely positive metric structures as in “usual” QM. The square-root branching behavior is easily seen by passing from the linear eigenvalue problems for the 2×2 -operator matrices H and $\hat{H}[\alpha]$ of Eqs. (9) and (12),

$$(H - E)\psi = 0, \quad (\hat{H}[\alpha] - \lambda)\phi = 0,$$

via substitutions

$$\psi = \begin{pmatrix} \psi_+ \\ -\frac{1}{H_{+-}}[H_{++} - E]\psi_+ \end{pmatrix}, \quad \phi = \begin{pmatrix} \phi_1 \\ \frac{1}{\alpha}[Q(1) + \lambda]\phi_1 \end{pmatrix}$$

to the equivalent quadratic operator pencils

$$\left\{ (H_{--} - E) \frac{1}{H_{+-}} (H_{++} - E) - H_{-+} \right\} \psi_+ = 0,$$

$$\left\{ (Q[1] + \lambda) \frac{1}{\alpha} (Q[1] + \lambda) - Q[\alpha] \right\} \phi_1 = 0.$$

Both pencils are of the same generic operator type

$$L[\lambda]\psi = [A_2\lambda^2 + A_1\lambda + A_0]\psi = 0$$

with a scalar product

$$(\psi, L[\lambda]\psi) = a_2\lambda^2 + a_1\lambda + a_0 = 0, \quad a_j := (\psi, A_j\psi)$$

which can be used to deduce the local square-root branching behavior of the spectrum

$$\lambda_{1,2} = \frac{1}{2a_2} (-a_1 \pm \sqrt{a_1^2 - 4a_0a_2}).$$

A typical α^2 -dynamo spectrum with a large number of real-to-complex transitions is presented in Fig. 1 (see also Refs. 14 and 35). These crossings with real-to-complex transition occur at exceptional points (in the sense of Kato³⁶) of (square root) branching type^{37,38} and the corresponding eigenvalues have geometric multiplicity one and algebraic multiplicity two.¹⁴ In contrast, crossings without real-to-complex transitions are of the same type as level crossings in Hermitian systems¹¹—with geometric and algebraic multiplicity two.³⁹ Finally, we note that although locally crossings with real-to-complex transitions occur, in general, only between two spectral branches, globally much more branches are involved in mutual crossings (see Fig. 1). This reflects the fact that in general the spectrum forms a multisheet Riemann surface over the parameter space of the theory (see, e.g., Refs. 33, 34, and 40).

In the next section, we will analyze the spectral behavior of a \mathcal{PT} -symmetric interpolation model where we will find a similar rich structure of real-to-complex transitions as for the α^2 -dynamo.

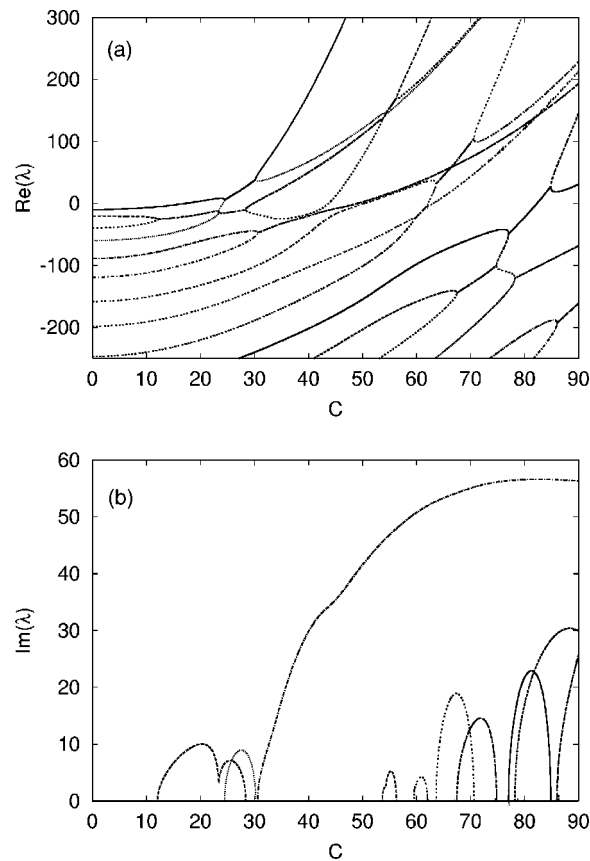


FIG. 1. Real and imaginary components of the α^2 -dynamo spectrum as functions of the scale factor C of an α -profile $\alpha(r) = C \times (1 - 26.09 \times r^2 + 53.64 \times r^3 - 28.22 \times r^4)$ in the case of angular mode number $l=1$ and physically realistic boundary conditions (13). The concrete coefficients in the quartic polynomial $\alpha(r)$ have their origin in numerical simulations of the field reversal dynamics (see Ref. 30). Only the imaginary components with $\Im\lambda \geq 0$ are shown. The complex conjugate ($\Im\lambda \leq 0$)-components are omitted for sake of brevity.

III. \mathcal{PT} -SYMMETRIC INTERPOLATION BETWEEN SQUARE WELL AND HARMONIC OSCILLATOR

In Schrödinger-type models (1) over the open real line $x \in (-\infty, \infty)$ a \mathcal{PT} SQM-related separation of the “physical” and “unphysical” domains is, in general, a mathematically highly nontrivial problem. Its resolution requires a fairly subtle and rigorous mathematical argumentation.^{16,29} A typical result of the WKB analysis of Ref. 1 was that in a half-open interval of $\nu \in [0, 2)$ the energies remain real and that the \mathcal{PT} -symmetry of the wave functions remains unbroken. In parallel, a characteristic unphysical behavior of the system (1) has been found in the half-open interval of $\nu \in [-1, 0)$, where at any $\nu < 0$ all the sufficiently high-lying energies E_n with $n > n_0(\nu)$ “decay” in complex-conjugate pairs, $\Im E_n \neq 0$. Moreover, the spectrum becomes empty in the Herbst–Hamiltonian limit of the leftmost $\nu = -1$.¹

A. Toy model \mathcal{PT} -symmetric differential equation

In the present section, we are going to extend the consideration of the Schrödinger-type system (1) to exponents from the interval $\nu \in [-2, 0]$. The endpoints of this interval correspond to the purely real-valued Hermitian-system spectra of a freely moving particle with shifted off-set energy (for $\nu = -2$) and a harmonic oscillator (for $\nu = 0$). For the exponents $\nu \in (-2, 0)$ we expect a phase of spontaneously broken \mathcal{PT} -symmetry with an involved picture of real-to-complex spectral phase transitions.

In order to keep the numerical analysis sufficiently simple and robust, we assume the system located in a square well (box) of *finite* width $2b < \infty$ and Dirichlet boundary conditions imposed at the walls, $\psi(x = \pm b) = 0$, i.e., we introduce an IR cutoff at the low-energy end of the spectrum (various aspects of square-well-related PTSQM setups have been earlier considered, e.g., in Refs. 11, 41, and 42). This enables us to rescale Eq. (1) to the equivalent equation

$$[-\partial_y^2 + G y^2 (iy)^\nu] \psi[x(y)] = \mu(E) \psi[x(y)] \quad (18)$$

with parameter-independent boundary conditions

$$\psi[x(\pm 1)] = 0, \quad (19)$$

but rescaled coupling constant and energy

$$G = g b^{4+\nu}, \quad \mu(E) = b^2 E.$$

In this notation, the original bound-state problem (1) with asymptotic Dirichlet boundary conditions at $x \rightarrow \pm\infty$ is replaced by the equivalent new problem defined within a fixed finite interval $[-1, 1]$. In the limit of very small $b \approx 0$ the potential term becomes negligible, $G \approx 0$, and the interaction degenerates to an infinitely deep square well (box) at all ν . A completely similar situation occurs for systems with any nonvanishing finite b , but very small exponents, $\nu \approx -2$. In both extremal cases the problem remains exactly solvable. The original Bender–Boettcher problem corresponds to the strong-coupling limit, $G \rightarrow \infty$, $b \rightarrow \infty$, with g hold fixed, $g = G b^{-4-\nu} = \text{const}$.

For finite coupling constants $0 < G < \infty$ one expects the energy spectrum to be divided into the following three sectors: into a low-energy sector with states which are involved in real-to-complex phase transitions, into an intermediate sector, where the ν -dependent energies still remain real, and into a high-energy sector with almost ν -independent purely real eigenvalues whose states experience only a small perturbations from the complex interaction term. The division into low energy and intermediate-and-high energy sectors has been qualitatively described in a recent paper¹¹ by Langer and Tretter who considered a square well model with an arbitrary \mathcal{PT} -symmetric potential V as perturbation. Starting from the energy spectrum of the empty square well, $\mu_k = k^2 \pi^2 / 4$, $k = 1, 2, \dots$, they showed that there are no real-to-complex phase transitions for levels $k > k_s$ with k_s as the lowest level satisfying the supremum bound $\|V\|_\infty < (2k_s + 1) \pi^2 / 8$. In case of our model with potential $V(y) = g b^{4+\nu} y^2 (iy)^\nu$ the supremum norm (see, e.g., Ref. 43) reads (for $\nu \geq -2$)

$$\|V\|_\infty = \sup_{y \in [-1, 1]} |V(y)| = |V(\pm 1)| = |g| b^{4+\nu}$$

so that it is ensured that there are no phase transitions for levels

$$k > k_s(b) > \frac{1}{2} \left[\frac{8}{\pi^2} |g| b^{4+\nu} - 1 \right]. \quad (20)$$

According to Ref. 11 it holds for the corresponding real eigenvalues μ_k , $|\mu_k - k^2 \pi^2 / 4| < |g| b^{4+\nu}$. The supremum bound is safe, but at the same time rather rough.⁴⁴ The subsequent exact numerical analysis shows that, depending on the concrete exponents ν , the real-to-complex phase transitions in the model (18) stop at much lower energy levels.

B. The emergence of $\Im E \neq 0$ on certain finite subintervals of $\nu \in (-2, 0)$

In the generic case with $\nu \in (-2, 0)$ and $b > 0$, we have solved Eqs. (18) and (19) numerically by means of a shooting technique with a fifth-order Runge–Kutta method, utilizing and adapting standard routines from numerical recipes.⁴⁵ The corresponding code had been validated extensively in earlier work by comparison with known analytical results and other numerical results in dynamo theory and quantum mechanics.

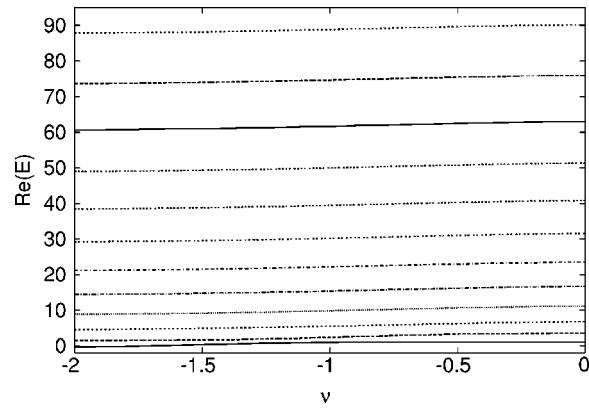


FIG. 2. Spectrum of the \mathcal{PT} -symmetric interpolation Hamiltonian $H = -\partial_x^2 + x^2(ix)^\nu$ as function of the exponent ν for the cutoff length $b=2$. All eigenvalues are real and almost independent of ν . The spectrum is only slightly deviating from that of an empty square well.

A sample of the results of such a study is depicted in Figs. 2–6, where we have chosen $g = 1$ and displayed the first few energy levels $E(\nu)$ over the entire interval $\nu \in (-2, 0)$ for the sequence of values $b=2, 4, 6, 7$. The important results of this numerical experiment are the following:

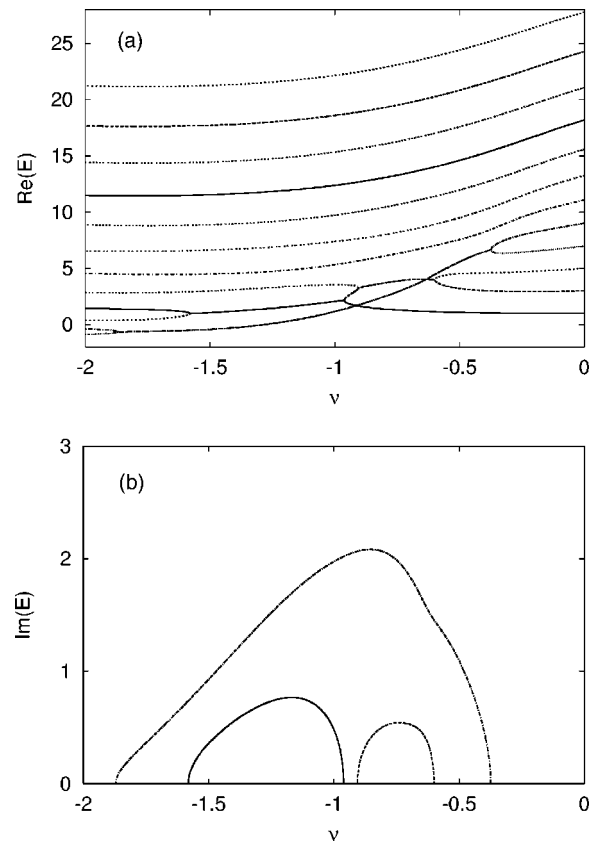
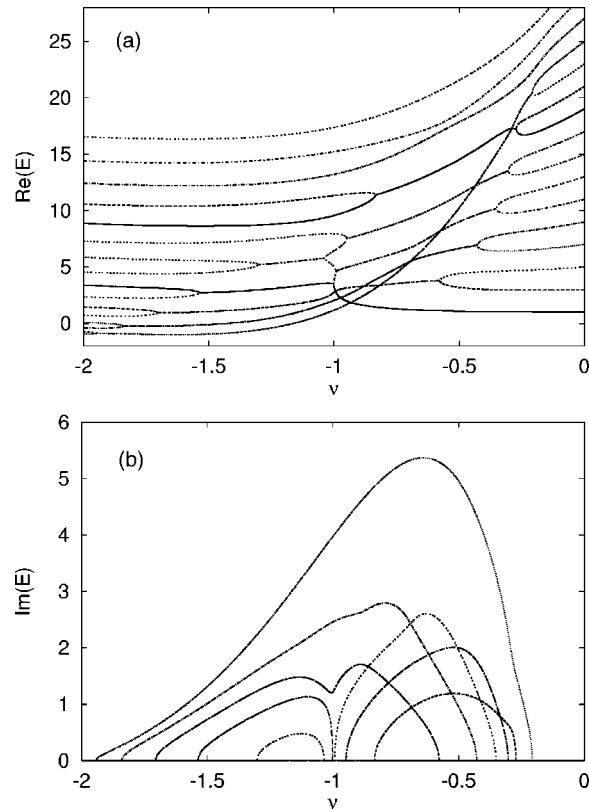


FIG. 3. Real and imaginary components of the spectrum in the case of a cutoff length $b=4$ [complex conjugate ($\Im\lambda \leq 0$) components omitted, as well as further higher lying levels without real-to-complex transitions]. The low-energy sector with its multiple real-to-complex transitions starts to form.

FIG. 4. Spectrum for a cutoff length $b=6$.

- (i) At all sufficiently small b , as sampled in Fig. 2, the energy spectrum exhibits a more or less ν -independent square-well form.
- (ii) At not too large b the spectrum, as sampled in Fig. 3, proves clearly separated into the high-lying part (where the energies still preserve their approximate ν independence), an intermediate perturbative part (where the perceivably ν -dependent energies still remain all real) and the low-lying part (where one encounters the first real-to-complex phase transitions).
- (iii) The actual lowest level numbers $k_c(b)$ (critical level numbers) of the modes which are not involved in real-to-complex transitions lie much below the safe supremum bounds $k_s(b)$ of inequality (20). Choosing, for example, the exponents $\nu=-1/2$ and $\nu=-3/2$ we read off that

$$\nu = -1/2, \quad b = \begin{cases} 2 \\ 4 \\ 6 \\ 7 \end{cases}, \quad k_s(b) > \begin{cases} 4.08 \\ 51.4 \\ 213 \\ 367 \end{cases}, \quad k_c(b) = \begin{cases} 1 \\ 6 \\ 14 \\ 22 \end{cases},$$

$$\nu = -3/2, \quad b = \begin{cases} 2 \\ 4 \\ 6 \\ 7 \end{cases}, \quad k_s(b) > \begin{cases} 1.79 \\ 12.5 \\ 35.2 \\ 52.1 \end{cases}, \quad k_c(b) = \begin{cases} 1 \\ 5 \\ 9 \\ 11 \end{cases}.$$

- (iv) Starting from the “intermediate width” region, sampled at $b=6$ in Fig. 4, we find that the *left-hand half* of the picture exhibits a clear transition from the slightly non-Hermitian

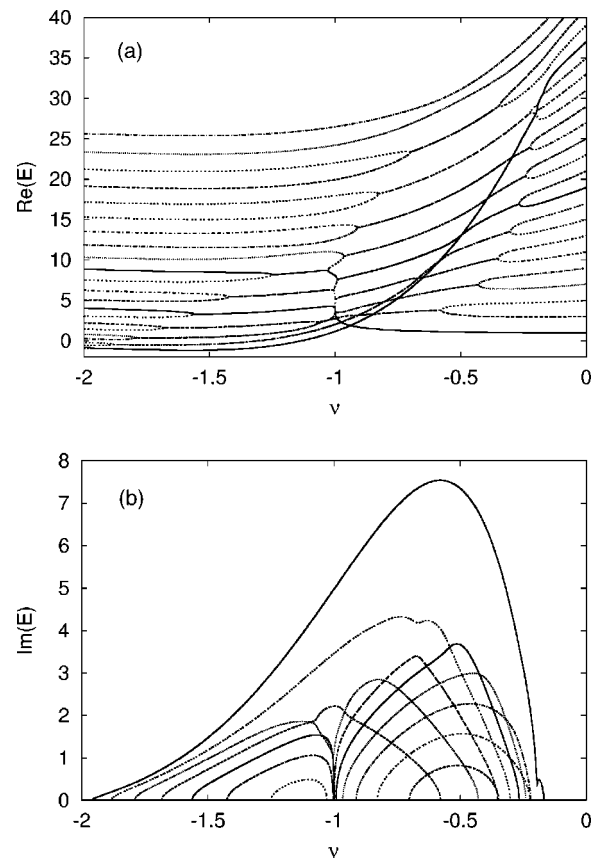


FIG. 5. At a cutoff length $b=7$ the generic structure of the spectrum is clearly visible. The weblike pattern of the real components (a) contains purely real branches in the vicinity of the left ($\nu=-2$) and right ($\nu=0$) endpoints of the considered interval as well as a chain of purely real intermediate segments in the vicinity of $\nu=-1$. (See Fig. 6 for a detailed view.) The increasing number of imaginary components (b) with high gradients $|\partial_\nu E(\nu \approx -1)| \gg 1$ which accumulate in the vicinity of $\nu=-1$ are first indications of the formation of a local spectral singularity at $\nu=-1$.

square well regime (with the higher energies all real) to its more strongly non-Hermitian extension where for all exponents ν not too distant from $\nu=-2$ the purely imaginary and finite component of the potential resembles the spatially antisymmetric part of the exactly solvable \mathcal{PT} -symmetric Heavyside step potential within a square well considered in Ref. 41. This explains why in Figs. 3–5 the continuing decrease of ν makes the respective two or three lowest pairs of the energies merge and complexify.

- (v) At “sufficiently large” cutoffs b , all the *real* low-lying energies depicted in the *right-hand halves* of Figs. 4 and 5 obviously stabilize and approach the $b \rightarrow \infty$ limiting pattern as published in Refs. 1 and 16. In particular, we see that the ground-state energy remains real and that it starts growing more quickly only when the values of ν move down and closer to the Herbst limit of $\nu \rightarrow -1^+$. We observe that in a more appropriate way this growing real branch should be interpreted as a special type of ladder-shaped merger of intermediate real segments which actually correspond to level pairs with higher mode numbers. A zoomed view on this peculiarity is presented in Fig. 6, where it is clearly visible that a chain of exceptional points is located on this branch with alternating complex-valued segments branching off to the left and to the right. These segments fit, after further complex-to-real transitions, to the real eigenvalues of the $\nu \rightarrow 0$ and $\nu \rightarrow -2$ limit models.
- (vi) When the cutoff b is increased the following simultaneous changes in the spectrum can be observed. In the upper low-energy region with $\nu > -1$ step by step more and more level pairs become twisted into the complex sector. With a “slight delay in b ” and at $\nu < -1$ the lower of the twisted levels undergo a second pairwise real-to-complex transition with the

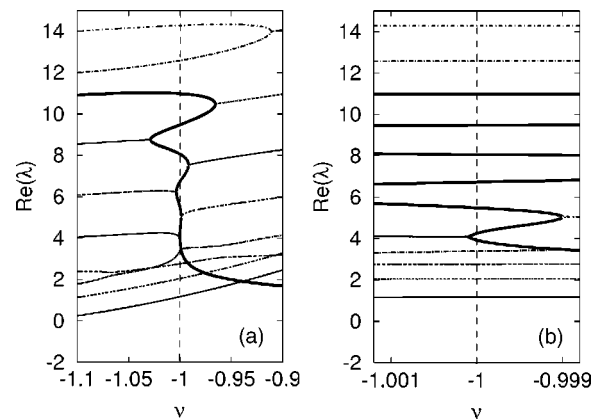


FIG. 6. The purely real curve (high-lighted fat) in the vicinity of $\nu=-1$ (cutoff length $b=7$) is formed by intermediate real segments between complex valued segments which branch off to the left and to the right. This leads to a ladderlike structure with exceptional points as nodes. The zoomed picture in (b) shows that the “oscillations” of the real curve about the line $\nu=-1$ persist also at its lower end, but with strongly reduced “amplitude.” When the cutoff is slightly increased to $b \geq 7$ the lowest exceptional (real-to-complex transition) point (b) will cross the line $\nu=-1$ and will in the region $\nu > -1$ coalesce with the other (nearest) exceptional point. As a result, one intermediate segment will be removed from the real curve and a purely complex-valued branch pair will smoothly tend from “far left” ($\nu < -1$) to “far right” ($\nu > -1$)—similar to the lower lying purely complex branches visible in the graphics.

levels below them. A sort of web structure is forming with a purely real branch remaining between the left ($\nu < -1$) and right ($\nu > -1$) purely complex (twisted) spectral regions. The complex-valued level pairs are branching off from the real branch forming a ladder-shaped structure. At the low-energy end of this ladder a second process occurs. The left ($\nu < -1$) complex level pairs are passing the line $\nu=-1$ and move to the right of it. There, at some $\nu > -1$ the corresponding exceptional point merges with an exceptional point of a right branch. As a result, one of the real segments between left and right off-branching levels disappears and a smooth complex-valued branch forms which extends over a large ν interval and whose imaginary components are increasing very fast when b is increased. It remains the real branch which becomes more and more vertical whereas the complex branch is not intersecting with it (the real component of the complex branch is coinciding at one point with the real branch but the imaginary components are not coinciding).

Analyzing the sequence of Figs. 2–6 we observe that, when the cutoff b is increased, a rather special (and seemingly inextricable) branch pattern of real and complex eigenvalues is forming in the vicinity of the exponent $\nu=-1$. [The phenomenon may be generic since in Ref. 46, the “wiggly upwards” spectral pattern has also been detected for a very different one-parametric family of asymptotically exponential \mathcal{PT} -symmetric potentials $V(x) = -(i \sinh x)^\beta$ near the Herbst-type exponent $\beta=1$.] The extreme steepness of an increasing number of imaginary branches and their accumulation at $\nu=-1$ (see Figs. 4 and 5) as well as the occurrence of the almost vertical real branch (Fig. 6) are indicating the formation of a local spectral singularity with $\partial_\nu E|_{\nu=-1} \rightarrow \pm\infty$ at the (almost) vertical segments of the real-valued branch as well as on the imaginary branches close to the exceptional points of the “ladder” structure. From the figures it is not at all obvious how this pattern is compatible with the Herbst limit of an empty spectrum for $b \rightarrow \infty$ at $\nu=-1$. We will resolve this interesting puzzle in the next section.

IV. THE HERBST LIMIT AND ITS RELATION TO THE SQUIRE EQUATION OF HYDRODYNAMICS

In Ref. 15 it was shown by Herbst that the spectrum of a Hamiltonian with imaginary linear potential (imaginary homogeneous electric field) over the real line $x \in \mathbb{R}$ is empty. The differential expression of the corresponding operator coincides with that of the \mathcal{PT} -symmetric Schrödinger-type equation (18) with exponent $\nu=-1$,

$$[-\partial_y^2 - igb^3y]\psi(y) = b^2E\psi(y), \quad \psi(y = \pm 1) = 0. \quad (21)$$

The only difference of (21) compared to the Herbst model is in the Dirichlet boundary conditions at $y = \pm 1$ which restrict the system to a box (square well). Due to this analogy and for sake of brevity, we will call the model (21) a ‘‘Herbst box.’’

We start our consideration by noticing that Eq. (21) and the spectral function $\mu(b, E) = b^2E$ are invariant under the rescaling $b \mapsto g^{-1/3}b$, $E \mapsto g^{2/3}E$ so that henceforth we can set $g = 1$, without loss of generality. The corresponding Herbst box Hamiltonian we denote as

$$H_{Hb}(b) := -\partial_y^2 - ib^3y. \quad (22)$$

Equation (21) itself is of Airy type and its solutions can be expressed as

$$\psi(y) = C_1 A_1[\xi(y)] + C_2 A_2[\xi(y)],$$

$$\xi(y) := e^{i(\pi/3)}[-iby - E],$$

where $C_{1,2} = \text{const}$, and $A_1(\xi)$, $A_2(\xi)$ are any two of the Airy functions $\text{Ai}(\xi)$, $\text{Ai}(q\xi)$, $\text{Ai}(q^2\xi)$ with $q := e^{i2\pi/3}$. As usual, the boundary conditions lead to a characteristic determinant which defines the spectrum of the eigenvalue problem. In case of Eq. (21), it reads

$$\Delta(E) = A_1(\xi_+)A_2(\xi_-) - A_1(\xi_-)A_2(\xi_+) = 0, \quad \xi_{\pm} := \xi(y = \pm 1). \quad (23)$$

Characteristic determinants of this type (built over Airy functions) have been intensively studied since 1995 in a paper series of Stepin^{47,48} and Shkalikov *et al.*⁴⁹ (for related work see also Ref. 50) on the spectral properties of the Squire equation of hydrodynamics (the corresponding physical background can be found, e.g., in Refs. 51 and 52)

$$H_{\text{Sq}}(\varepsilon) := i\varepsilon\partial_y^2 + y, \quad (H_{\text{Sq}} - \lambda)\chi = 0, \quad \chi(y = \pm 1) = 0, \quad \varepsilon := (\tilde{\alpha}R)^{-1}. \quad (24)$$

Before we make the (obviously existing) relation of this model to the Herbst box model explicit, we briefly review a few of its properties.

The Squire equation (24) describes the normal vorticity of a plane Couette flow with linear velocity profile. The parameter $\tilde{\alpha} > 0$ denotes a real-valued wave number which originates from the decomposition of a two-dimensional flow perturbation,

$$\Psi(x, y, t) = \chi(y)e^{i\tilde{\alpha}(x - \lambda t)},$$

$R > 0$ is the Reynolds number and ε —the viscosity. The spectrum of H_{Sq} was found to have a Y-shaped form.^{48,49,51} All the eigenvalues are located in a close vicinity of the three segments $(1, -i/\sqrt{3}]$, $(-1, -i/\sqrt{3}]$, $[-i/\sqrt{3}, -i\infty)$. In the limit of large $R \rightarrow \infty$, $\tilde{\alpha} \geq 1$ and correspondingly small $\varepsilon \rightarrow 0^+$ the eigenvalue problem (24) turns into a singular perturbation problem and its eigenvalues show a remarkable limiting behavior. For $\varepsilon \rightarrow 0^+$, more and more eigenvalues ‘‘move in’’ from $-i\infty$ along the line $[-i/\sqrt{3}, -i\infty)$, merge pairwise in the vicinity of the point $-i/\sqrt{3}$, and depart then (again pairwise) to move symmetrically along the segments $[1, -i/\sqrt{3}]$, $[-1, -i/\sqrt{3}]$ and to ‘‘fill’’ them step by step—leaving the Y-shape invariant. The process was described in Ref. 48 as a special type of transition from a discrete spectrum to a continuous one. Explicitly, the following asymptotic estimates were found in Refs. 48 and 49:

$$\lambda_n \sim -i\varepsilon \frac{\pi^2 n^2}{4} \in [-i/\sqrt{3}, -i\infty), \quad n \rightarrow \infty, \quad (25)$$

$$\lambda_n^{\pm} \sim \pm 1 \pm \varepsilon^{1/3} s_n e^{\pm i\pi/6} \in (\pm 1, -i/\sqrt{3}], \quad \varepsilon \rightarrow 0^+, \quad (26)$$

where s_n are the zeros of the Airy function

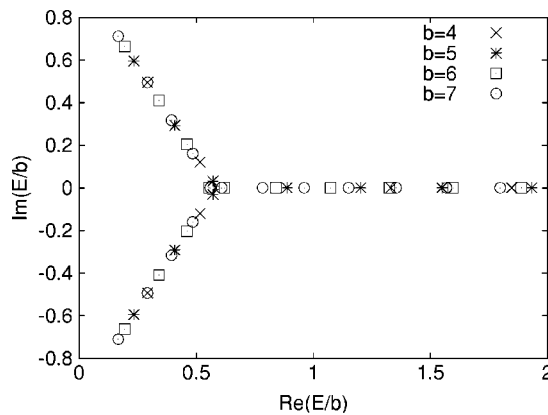


FIG. 7. The rescaled Herbst-box spectrum $E/b = i\lambda(\epsilon = b^{-3})$ coincides with the Wick-rotated Y-shaped spectrum of the Squire operator $H_{\text{Sq}}(\epsilon)$.

$$\text{Ai}(s_n) = 0, \quad s_n \in \mathbb{R}_-$$

One clearly sees that the smaller ϵ is chosen the smaller the distances between the eigenvalues become—leading in the limit $\epsilon \rightarrow 0$ to a quasicontinuous spectrum.

Noticing that the pairwise merging and splitting (level crossing) of the eigenvalues occurs at $\lambda^+ \sim \lambda^- \sim -i/\sqrt{3}$, it is easy to estimate that the value ϵ_n , for which this crossing is connected with the n th Airy function root s_n , is given by

$$\epsilon_n^{1/3} \sim \frac{2}{|s_n|\sqrt{3}}. \quad (27)$$

Let us utilize the above results now for the Herbst-box model. A simple comparison of the eigenvalue problems (21) (for $g=1$) and (24) shows that these problems may be made coinciding if one sets

$$i\epsilon^{-1}[H_{\text{Sq}}(\epsilon) - \lambda]\chi(y) \stackrel{!}{=} \mathcal{P}[H_{\text{Hb}}(b) - b^2E]\mathcal{P}[\mathcal{P}\psi(y)] = 0$$

and identifies

$$b^3 = \epsilon^{-1}, \quad E = ib\lambda, \quad \mathcal{P}H_{\text{Hb}}(b)\mathcal{P} = i\epsilon^{-1}H_{\text{Sq}}(\epsilon), \quad \mathcal{P}\psi(y) = \chi(y). \quad (28)$$

This means that the two models are related by the combined action of a rescaling, a Wick rotation and a coordinate reflection \mathcal{P} .

With the help of the estimates (25) and (26) it is now an easy task to explain the behavior of the Herbst-box spectrum $E(b)$.

- (i) The rescaled spectrum $E(b)/b = i\lambda(\epsilon = b^{-3})$ (shown in Fig. 7) is simply the Wick-rotated version of the original shape-invariant “Y” of the Squire operator $H_{\text{Sq}}(\epsilon)$. With increasing $b = \epsilon^{-1/3}$ more and more eigenvalues “move in” from $+\infty$ and “fill” the two complex conjugate branches $(i, 1/\sqrt{3}]$, $(-i, 1/\sqrt{3}]$ of the “Y” as well as the half-line $[1/\sqrt{3}, +\infty)$ —in a similar way as in the original $\lambda(\epsilon \rightarrow 0)$ limit. For $b \rightarrow \infty$ the spectrum becomes quasicontinuous on the rotated “Y.”
- (ii) Due to the shape invariance of $E(b)/b$, the spectrum $E(b) = ib\lambda(b^{-3})$ itself inflates when b increases. It is located in the close vicinity of the segments $(ib, b/\sqrt{3}]$, $(-ib, b/\sqrt{3}]$, $[b/\sqrt{3}, +\infty)$ and moves with $b \rightarrow \infty$ to infinity—leaving (for sufficiently high b) an empty region at any fixed finite distance from the origin of the spectral E plane. Hence, we find (as required) that for $b \rightarrow \infty$ the Herbst-box spectrum turns into the empty spectrum of the original Herbst model over the real line \mathbb{R} .

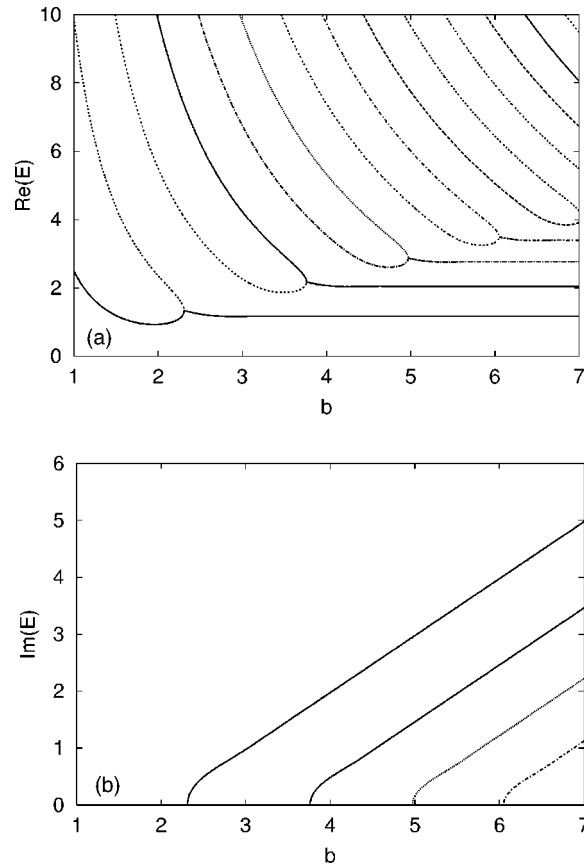


FIG. 8. Real and imaginary components of the Herbst-box spectrum as functions of the cutoff length b [complex conjugate ($\Im\lambda \leq 0$)-components omitted]. The asymptotical behavior of the complex-valued branches is clearly visible (constant real components and linear b dependence of the imaginary components).

(iii) For finite b , the asymptotic estimates (25) and (26) map into

$$E_k \sim \frac{\pi^2 k^2}{4b^2} \in b \times [1/\sqrt{3}, +\infty), \quad k \rightarrow \infty, \quad (29)$$

$$E_n^\pm \sim \pm ib \pm is_n e^{\pm i\pi/6} \in b \times (\pm i, 1/\sqrt{3}], \quad b \rightarrow \infty, \quad (30)$$

and we identify (29) as the pure square well spectrum

$$\mu(b, E_k) = b^2 E_k \sim \pi^2 k^2 / 4 \in b^3 \times [1/\sqrt{3}, +\infty) \quad (31)$$

of the high-energy sector which is almost not affected by the \mathcal{PT} -symmetric interaction. In contrast, the low-energy sector described by (30) shows a purely linear scaling behavior of the imaginary energy components $\Im E_n^\pm$, whereas the real components remain asymptotically fixed when b increases. This situation is also clearly visible from the numerical results presented in Fig. 8. The graphics of the equivalent spectrum $\mu(b, E)$, depicted in Fig. 9, provides a complementary description and shows how (for increasing b) the b -independent eigenvalues $\mu(b, E_k)$ of Eq. (31) leave the high-energy sector, obtain an explicit b dependence in the intermediate-energy sector and finally coalesce and split into complex conjugate pairs.

(iv) From the form of the spectral branches on the E plane (rotated “Y”) it is clear that the level crossings in the vicinity of $E \sim b/\sqrt{3}$ correspond to the typical real-to-complex phase tran-

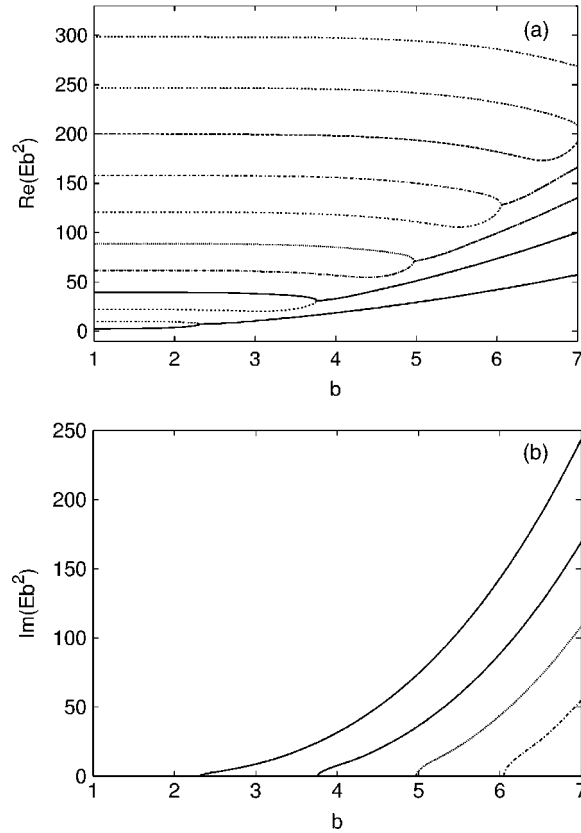


FIG. 9. The rescaled Herbst-box spectrum $\mu(b, E) = b^2 E$ allows a complementary view on the transition from the high-energy sector to the intermediate and low-energy sector.

sitions of \mathcal{PT} -symmetric models in Krein spaces. With the help of relation (27) the cutoff-scales b_n and positions E_n of the level crossings can be roughly estimated as

$$b_n \sim |s_n| \sqrt{3}/2, \quad E_n \sim |s_n|/2. \quad (32)$$

One can use the explicit values of these b_n ($b_1 \approx 2.02$, $b_2 \approx 3.54$, $b_3 \approx 4.78$, $b_4 \approx 5.88$, $b_5 \approx 6.87$, $b_6 \approx 7.81, \dots$), to roughly derive the number of the lowest uncrossed modes in the cases $b=2, 4, 6, 7$. For $b=2, 4, 6$ the result exactly coincides with the level crossing pattern shown (at $\nu=-1$) in Figs. 2–4, whereas the value b_5 is clearly smaller than the actual transition value $b_{5(c)}$ for which according to Figs. 6(b) and 8 holds $b_{5(c)} \gtrsim 7$. For completeness, we note that the asymptotic approximation⁴⁸ of the Airy function roots

$$|s_n| = \left[\frac{3\pi}{2} \left(n - \frac{1}{4} \right) \right]^{2/3} + O(n^{-4/3}), \quad n \rightarrow \infty$$

together with (32) yields the following rough estimate for the lowest purely real-valued mode:

$$k_a > \frac{4}{3\pi} \left(\frac{2}{\sqrt{3}} b \right)^{3/2} + \frac{1}{2}.$$

The scaling dimension $\kappa_a = 3/2$ of this bound is only one-half of the scaling dimension $\kappa_s = 4 + \nu = 3$ of the corresponding supremum bound (20). The exact positions of the level crossing points are given by the multiple roots of the characteristic determinant, $\Delta(E)$

$=0$, $\partial_E \Delta(E)=0$. This equation system can be simplified via Wronskian $W[A_1(\cdot), A_2(\cdot)]$ to yield the conditions

$$A_{1,2}(\xi_+) = \pm A_{1,2}(\xi_-)$$

(see Ref. 48 for the details). Plugging the numerical results from the eigenvalue solver into this equation with $A_{1,2}(\xi)$ chosen as in Ref. 48, $A_1(\xi) := \text{Ai}(\xi)$, $A_2(\xi) := \text{Ai}(q^2 \xi)$, selects the condition $A_{1,2}(\xi_+) = A_{1,2}(\xi_-)$ and satisfies it within numerical working precision. For the same data holds $A_{1,2}(\xi_+) \neq -A_{1,2}(\xi_-)$.

- (v) The spectral behavior $E(b)$ for increasing cutoff b can be summarized as follows. At the beginning, the real eigenvalues from the high-energy sector decrease as $E_k \sim \pi^2 k^2 / (4b^2)$ —moving into the intermediate energy region. When b approaches $b_n \sim |s_n| \sqrt{3}/2$ from below, the real eigenvalues $\{E_{2n-1}, E_{2n}\}$ (corresponding to a pair of positive and negative Krein space states¹¹) coalesce at $E_{2n-1} \sim E_{2n} \sim |s_n|/2$ and a real-to-complex transition occurs $\{E_{2n-1}, E_{2n}\} \rightarrow \{E_n^+, E_n^-\}$. When b is further increased the real energy components remain fixed $\Re E_n^\pm \approx |s_n|/2$ [see Fig. 8(a)], whereas the imaginary components blow up linearly along the asymptotes $\Im E_n^\pm \sim \pm b \pm s_n \sqrt{3}/2$ [Fig. 8(b)].

Let us, for finite b , relate the obtained Herbst-box results to the spectral behavior of the \mathcal{PT} -symmetric interpolation model of the preceding section. Apart from the obvious one-to-one correspondence of the high-energy sectors [see (31)], a clear identification is immediately possible for those Herbst-box eigenvalues which are close to the imaginary axis and which have the largest imaginary components. These eigenvalues are located on the branches with the largest imaginary components in Figs. 3–5 (which stay complex when ν passes through the Herbst-box value $\nu=-1$). It is clearly visible from these figures that, for increasing b , the imaginary components are blowing up, whereas the real components remain asymptotically constant.

So far, we have found a clear correspondence for those regions on the Herbst-box “Y” which are located away from the center of the “Y” with its real-to-complex phase transitions. A more subtle situation occurs in the vicinity of this center. The corresponding Herbst box eigenvalues will map into points located close to (or on) the forming (almost) vertical segment of the purely real branch depicted in Fig. 6. From the zoomed graphics in Fig. 6(b) we observe that the purely real and almost vertical branch of the interpolation model “oscillates” around the Herbst-box line at $\nu=-1$ with strongly decreasing “amplitude” to its low-energy part. With increasing b this “decreasing amplitude” effect becomes stronger and the “oscillations” are only traceable with the help of an appropriately increased zooming scale. Nevertheless, it can be read off that the real-to-complex transition of the Herbst-box spectrum follows qualitatively the same scheme for any finite b . The real eigenvalues of the Herbst box are all located on the purely real branch of the interpolation model and the real-to-complex transition occurs when the lowest exceptional point on this branch moves from the left sector $\nu < -1$ through the Herbst-box value $\nu=-1$ into the right sector $\nu > -1$ —to coalesce afterwards with the next higher exceptional point from the right sector. With this passing of the left-sector exceptional point through the line $\nu=-1$ the Herbst-box eigenvalues become pairwise complex conjugate with strongly increasing imaginary components [due to the asymptotically diverging gradient $\partial_\nu E(b \rightarrow \infty)|_{\nu \approx -1} \rightarrow \pm \infty$]. The real-to-complex transition with subsequently increasing imaginary components are illustrated in Fig. 10.

Finally, we note that in the limit $b \rightarrow \infty$, the lowest-lying intersection of the purely real branch with the Herbst-box line $\nu=-1$ moves away to infinity like $b/\sqrt{3}$ (the lower bound of the real segment $[b/\sqrt{3}, \infty)$ of the Herbst-box “Y”) so that the real branch itself remains for any finite energy in the right sector $\nu > -1$ —approaching the Herbst-box line asymptotically. This reproduces the earlier observations of Refs. 1 and 16 for the spectrum of the Bender–Boettcher problem over the real line. Additionally, our Herbst-box results predict for this problem diverging imaginary components at $\nu=-1$: $|\Im E(b \rightarrow \infty, \nu \rightarrow -1)| \rightarrow \infty$. Taking these observations together we once more see that in the limit $b \rightarrow \infty$ a spectral singularity is forming at $\nu=-1$ with $|E(b \rightarrow \infty, \nu \rightarrow -1)| \rightarrow \infty$, $|\partial_\nu E(b \rightarrow \infty, \nu \rightarrow -1)| \rightarrow \infty$.

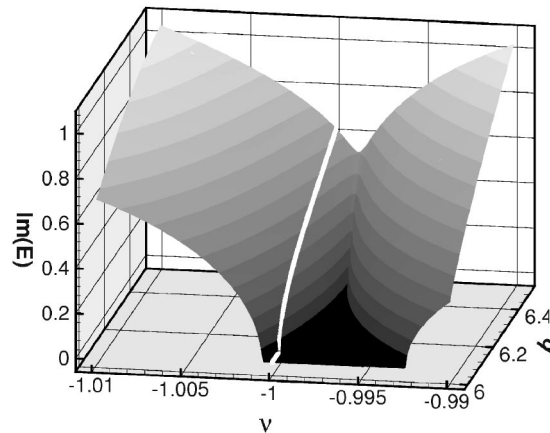


FIG. 10. Concrete example for the generic merging process of two complex-valued spectral branches (present here for $b < b_{\text{coal}} \approx 6.36$) into a single complex-valued branch for $b > b_{\text{coal}}$. The two exceptional (real-to-complex transition) points existing for $b < b_{\text{coal}}$ are located on the plane $(\nu, b, \Im E = 0)$ and coalesce at $b = b_{\text{coal}}$. The corresponding point $(\nu_{\text{coal}} \approx -0.9983 > -1, b_{\text{coal}} \approx 6.36, \Im E = 0)$ is the starting (cusp) point of a sharp “valley” of the nonvanishing imaginary component which steeply grows and smooths when $b > b_{\text{coal}}$ is further increased. The white curve marks the Herbst-box values. Before the two exceptional points coalesce, the left one of these points crosses the Herbst-box configuration at $(\nu = -1, b = b_c \approx 6.02, \Im E = 0)$ and a real-to-complex transition occurs for the Herbst-box model.

V. CONCLUSIONS

In the present paper we considered three models emerging in different physical setups, but which are closely related with each other by their underlying mathematical structure as spectral problems in Krein spaces. The models are a one-dimensional \mathcal{PT} -symmetric quantum mechanical interpolation setup defined over a square well of finite width $2b$, the spherically symmetric MHD α^2 -dynamo as well as the Squire equation of hydrodynamics. For the PTSQM model and the α^2 -dynamo we made their close relation transparent by transforming them into a 2×2 matrix operator representation with coinciding block structure of the Krein space metric (involution operator). In the case of the Squire equation we showed that the corresponding spectral problem is connected with a \mathcal{PT} -symmetric eigenvalue problem by a rescaling and Wick rotation. (It is clear that, apart from the Squire equation, there will exist other hydrodynamic equations which can be structurally identified as Wick-rotated \mathcal{PT} -symmetric systems in Krein spaces.)

Based on recent results on the spectrum of the Squire equation, we performed a qualitative analysis of the \mathcal{PT} -symmetric quantum mechanical interpolation model for arbitrary square well widths (cutoffs) $2b$. This allowed us to trace the emergence of the Herbst limit with its empty spectrum as a spectral singularity and to fit our results to those of the Bender–Boettcher equation over the real line. We obtained a rich structure of multiple spectral phase transitions from purely real eigenvalues to pairs of complex conjugate ones—as it was to expect for spectral problems in Krein spaces.

A deeper insight into the Herbst-box spectrum and a possible extension of the present results to \mathcal{PT} -symmetric Hamiltonians of the type $H_{M,N} = -\partial_x^2 + x^{2M}(ix)^N$, $M, N = 1, 2, 3, \dots$ over square wells can probably be achieved by representing the characteristic determinant $\Delta(E)$ in (23) via Hadamar product representation of the Airy functions⁵³ as a spectral determinant of Bethe-ansatz type^{16,29,54} and studying it by similar cocycle functional equations as in Ref. 55.

A question which was not touched in the present paper concerns the orthogonality of the Herbst-box eigenfunctions. For the Squire equation it is known that its eigenfunctions show a strong nonorthogonality^{47,51} (due to the non-normality of the Squire operator) for eigenvalues in the vicinity of the branch point center of the “Y” (pseudospectral techniques^{50,51,56} play an important role in this case). Our above considerations indicate on a link of this issue with the forming spectral singularity $|\partial_\nu E(\nu \approx -1, b \gg 1)| \gg 1$ in the vicinity of the almost vertical segments of the purely real branch in the spectrum of the \mathcal{PT} -symmetric interpolation model.

Finally, we would like to note two issues which seem of relevance for future considerations. The first one is in developing efficient mathematical tools to find the hypersurfaces in parameter space where spectral phase transitions of the real-to-complex type occur. [A two-step method similar in spirit was successfully used, e.g., in higher-dimensional gravitational models to obtain the stability regions in the moduli (parameter) space of these models (step one, find the critical hypersurfaces; step two, identify the stability/instability properties of the model aside from these hypersurfaces).⁵⁷] Knowing these hypersurfaces, one would know the boundaries which separate the parameter space regions with unbroken \mathcal{PT} -symmetry from regions with spontaneously broken \mathcal{PT} -symmetry. In case of α^2 -dynamos the corresponding knowledge would allow for a more precise prediction of configurations with tendency to magnetic field reversals. The second issue concerns methods for solving inverse spectral problems in Krein spaces. Such methods would be extremely helpful for the data analysis of the dynamo experiments which are planned for the near future at seven sites around the world.⁵⁸

ACKNOWLEDGMENTS

The authors thank G. Gerbeth, H. Langer, K.-H. Rädler, and C. Tretter for useful comments. The project was supported by the German Research Foundation DFG, Grant No. GE 682/12-2 (U.G., F.S.) and by GA AS ČR, Grant No. 1048302 (M.Z.).

APPENDIX: A FEW COMMENTS ON THE PHYSICS OF MHD α^2 -DYNAMOS

The dynamo operator $\hat{H}_l[\alpha]$ originates from the MHD mean-field induction equation (cf. Ref. 12)

$$\partial_t \mathbf{B} = \nabla \times (\alpha \mathbf{B}) + \nu_m \Delta \mathbf{B} \quad (\text{A1})$$

for the magnetic field \mathbf{B} . This equation results from averaging over small scale turbulences in the velocity field of the electrically conducting fluid (or plasma) which drives the dynamo. The helical turbulence function $\alpha(x)$ [also called α -profile (in general setups, α is not a scalar function but a tensor¹²)] encodes the net effect of the small scale physics on the large scale (mean) magnetic field \mathbf{B} . For certain topologically nontrivial helical velocity and \mathbf{B} -field configurations an inverse cascade effect occurs which induces an energy transfer from small-scale structures to large-scale structures (inverse to the energy transfer in usual turbulence cascades where the energy is pumped from large-scale structures into smaller structures until it finally dissipates and transforms into thermal energy). For sufficiently strong inverse cascade effects the advection term $\nabla \times (\alpha \mathbf{B})$ starts to dominate over the diffusion term $\nu_m \Delta \mathbf{B}$ (ν_m is the magnetic diffusivity) and the magnetic field strength starts to grow exponentially. This kinematic dynamo effect (growing \mathbf{B} field for a given velocity field of the fluid) is followed by a saturated dynamo regime where a balance between the dynamo effect and the back-reaction of the induced magnetic field on the velocity field (via Navier–Stokes equation) prevents a further growth of the field strength \mathbf{B} . For completeness, we note that an MHD dynamo is an open system in which part of the kinetic energy of the conducting fluid (or plasma) transforms into magnetic field energy.

The dynamo eigenvalue problem

$$\hat{H}_l[\alpha] \phi_{l,n} = \lambda_{l,n} \phi_{l,n}, \quad \phi_{l,n}(t) \sim \exp \lambda_{l,n} t \quad (\text{A2})$$

follows from the induction equation (A1) via a double decomposition: decomposing the \mathbf{B} field into poloidal and toroidal components (what leads to the two-component vector structure of $\phi_{l,n}$) and expanding them further into spherical harmonics. In the simplest (toy model) case of a spherically symmetric dynamo configuration the corresponding modes decouple completely and one arrives at the spherical l -mode projection (12) and (A2) (the subscript n denotes the radial mode number).

Up to now only a single exactly solvable α^2 -dynamo model is known—the model with constant α -profile.¹² Its spectrum is discrete, real,⁵⁹ bounded above and, depending on the value of

α , it is either completely negative (for α below a critical α_c : $\alpha < \alpha_c$) or it contains a finite number of positive eigenvalues $\lambda_{l,n} > 0$. The dynamo effect is dominated by these latter eigenmodes. In practice, it usually suffices to concentrate the analysis on the dominating upper most growing mode (or a few of the upper most modes) for dipole ($l=1$) and quadrupole ($l=2$) configurations. (There exist no “s-wave” α^2 -dynamos with $l=0$.^{12,13})

The spectral properties of the dynamo operator $\hat{H}_l[\alpha]$ are becoming much richer for inhomogeneous α -profiles $\alpha(r) \neq \text{const}$, when real-to-complex transitions occur—as discussed in Sec. II C and shown in Fig. 1.

- ¹C. M. Bender and S. Boettcher, Phys. Rev. Lett. **24**, 5243 (1998).
- ²C. M. Bender, S. Boettcher, and P. N. Meisinger, J. Math. Phys. **40**, 2201 (1999).
- ³M. Znojil, Phys. Lett. A **259**, 220 (1999); J. Phys. A **33**, 4203 (2000); M. Znojil, F. Cannata, B. Bagchi, and R. Roychoudhury, Phys. Lett. B **483**, 284 (2000).
- ⁴A. Mostafazadeh, J. Math. Phys. **43**, 205 (2002); **43**, 2814 (2002).
- ⁵A. Mostafazadeh, J. Math. Phys. **43**, 3944 (2002).
- ⁶C. M. Bender, D. C. Brody, and H. F. Jones, Phys. Rev. Lett. **89**, 270401 (2002).
- ⁷C. M. Bender, D. C. Brody, and H. F. Jones, Am. J. Phys. **71**, 1095 (2003).
- ⁸C. M. Bender, Czech. J. Phys. **54**, 13 (2004); **54**, 1027 (2004).
- ⁹T. Ya. Azizov and I. S. Iokhvidov, *Linear Operators in Spaces with an Indefinite Metric* (Wiley-Interscience, New York, 1989).
- ¹⁰A. Dijksma and H. Langer, “Operator theory and ordinary differential operators,” in *Lectures on Operator Theory and Its Applications*, edited by A. Böttcher *et al.*, Am. Math. Soc., Fields Institute Monographs, Vol. 3 (American Mathematical Society, Providence, RI, 1996), p. 75.
- ¹¹H. Langer and C. Tretter, Czech. J. Phys. **54**, 1113 (2004).
- ¹²H. K. Moffatt, *Magnetic Field Generation in Electrically Conducting Fluids* (Cambridge University Press, Cambridge, 1978); F. Krause and K.-H. Rädler, *Mean-Field Magnetohydrodynamics and Dynamo Theory* (Akademie-Verlag, Berlin and Pergamon Press, Oxford, 1980); Ya. B. Zeldovich, A. A. Ruzmaikin, and D. D. Sokoloff, *Magnetic Fields in Astrophysics* (Gordon and Breach, New York, 1983).
- ¹³U. Günther and F. Stefani, J. Math. Phys. **44**, 3097 (2003).
- ¹⁴U. Günther, F. Stefani and G. Gerbeth, Czech. J. Phys. **54**, 1075 (2004).
- ¹⁵I. Herbst, Commun. Math. Phys. **64**, 279 (1977).
- ¹⁶P. Dorey, C. Dunning, and R. Tateo, J. Phys. A **34**, 5679 (2001).
- ¹⁷C. M. Bender, Contemp. Phys. (to be published).
- ¹⁸M. Znojil, quant-ph/0103054v1.
- ¹⁹G. S. Japaridze, J. Phys. A **35**, 1709 (2002).
- ²⁰A. Messiah, *Quantum Mechanics* (North-Holland, Amsterdam, 1961).
- ²¹A. Mostafazadeh, Nucl. Phys. B **640**, 419 (2002).
- ²²C. M. Bender, P. N. Meisinger, and Q. Wang, J. Phys. A **36**, 6791 (2003).
- ²³A. Mostafazadeh, J. Phys. A **36**, 7081 (2003).
- ²⁴M. R. E. Proctor, Astron. Nachr. **298**, 19 (1977); Geophys. Astrophys. Fluid Dyn. **8**, 311 (1977); K.-H. Rädler, *ibid.* **20**, 191 (1982); K.-H. Rädler and U. Geppert, “Turbulent dynamo action in the high-conductivity limit: A hidden dynamo,” in *Workshop on Stellar Dynamos*, edited by M. Nunez and A. Ferriz-Mas, ASP Conference Series 178, 1999, p. 151.
- ²⁵A. de Souza Dutra and C. A. S. Almeida, Phys. Lett. A **275**, 25 (2000); B. Bagchi, P. Gorain, C. Quesne, and R. Roychoudhury, Mod. Phys. Lett. A **19**, 2765 (2004); Czech. J. Phys. **54**, 1019 (2004).
- ²⁶F. Kleefeld, hep-th/0408028; hep-th/0408097.
- ²⁷A. Mostafazadeh, J. Math. Phys. **43**, 6343 (2002); **44**, 943(E) (2003).
- ²⁸C. Dembowski *et al.*, Phys. Rev. Lett. **86**, 787 (2001); W. D. Heiss and H. L. Harney, Eur. Phys. J. D **17**, 149 (2001).
- ²⁹K. C. Shin, Commun. Math. Phys. **229**, 543 (2002).
- ³⁰F. Stefani and G. Gerbeth, Phys. Rev. Lett. **94**, 184506 (2005).
- ³¹R. T. Merrill, M. W. McElhinny, and P. L. McFadden, *The Magnetic Field of the Earth* (Academic, San Diego, 1996).
- ³²E. Covas, R. Tavakol, A. Tworkowski, and A. Brandenburg, Astron. Astrophys. **329**, 350 (1998); G. Rüdiger and R. Hollerbach, *The Magnetic Universe* (Wiley-VCH, Weinheim, 2004), p. 160.
- ³³C. M. Bender and T. T. Wu, Phys. Rev. **184**, 1231 (1969).
- ³⁴W. D. Heiss and W. H. Steeb, J. Math. Phys. **32**, 3003 (1991).
- ³⁵F. Stefani and G. Gerbeth, Phys. Rev. E **67**, 027302 (2003).
- ³⁶T. Kato, *Perturbation Theory for Linear Operators* (Springer, Berlin, 1966).
- ³⁷M. V. Berry, Czech. J. Phys. **54**, 1039 (2004).
- ³⁸W. D. Heiss, Czech. J. Phys. **54**, 1091 (2004).
- ³⁹M. V. Berry and M. Wilkinson, Proc. R. Soc. London, Ser. A **392**, 15 (1984).
- ⁴⁰A. Marshakov, *Seiberg–Witten Theory and Integrable Systems* (World Scientific, Singapore, 1999).
- ⁴¹M. Znojil, Phys. Lett. A **285**, 7 (2001); M. Znojil and G. Lévai, Mod. Phys. Lett. A **16**, 2273 (2001); M. Znojil, J. Math. Phys. **45**, 4418 (2004); A. Mostafazadeh and A. Batal, J. Phys. A **37**, 11645 (2004).
- ⁴²B. Bagchi, S. Mallik, and C. Quesne, Mod. Phys. Lett. A **17**, 1651 (2002); V. Jakubský and M. Znojil, Czech. J. Phys. **54**, 1101 (2004); M. Znojil, quant-ph/0410196.
- ⁴³M. Reed and B. Simon, *Methods of Modern Mathematical Physics, Vol. 1. Functional Analysis* (Academic, New York,

- 1972).
- ⁴⁴C. Tretter (private communication).
- ⁴⁵W. H. Press, S. A. Teukolsky, W. T. Vetterling, and B. F. Flannery, *Numerical Recipes* (Cambridge University Press, Cambridge, 1992).
- ⁴⁶F. M. Fernandez, R. Guardiola, J. Ros, and M. Znojil, *J. Phys. A* **32**, 3105 (1999).
- ⁴⁷S. A. Stepin, *Usp. Mat. Nauk* **50**, 219 (1995) [*Russ. Math. Surveys* **50**, 1311 (1995)]; **53**, 205 (1998) [**53**, 639 (1998)].
- ⁴⁸S. A. Stepin, *Fundam. Prikl. Mat. Mekh.* **3**, 1199 (1997) (Fundamental and Applied Mathematics), (in Russian), freely available under <http://www.emis.de/journals/FPM/eng/econtent.htm>
- ⁴⁹A. A. Shkalikov, *Math. Z.* **62**, 950 (1997) [*Math. Notes* **62**, 796 (1997)]; A. A. Shkalikov and S. N. Tumanov, *ibid.* **72**, 561 (2002) [**72**, 519 (2002)]; A. V. Dyachenko and A. A. Shkalikov, *Funkc. Anal. Priloz.* **36**, 71 (2002) [*Funct. Anal. Appl.* **36**, 228 (2002)]; A. A. Shkalikov, math-ph/0304030.
- ⁵⁰P. Redparth, *J. Diff. Eqns.* **177**, 307 (2001).
- ⁵¹S. C. Reddy, P. J. Schmid, and D. S. Henningson, *SIAM J. Appl. Math.* **53**, 15 (1993).
- ⁵²P. J. Schmid and D. S. Henningson, *Stability and Transition in Shear Flows* (Springer, New York, 2001).
- ⁵³E. P. Merkes and M. Salmassi, *Complex Variables, Theory Appl.* **33**, 207 (1997); M. Salmassi, *J. Math. Anal. Appl.* **240**, 574 (1999).
- ⁵⁴P. Dorey and R. Tateo, *J. Phys. A* **32**, L419 (1999); P. Dorey, A. Millican-Slater, and R. Tateo, *J. Phys. A* **38**, 1305 (2005); P. Dorey, C. Dunning, and R. Tateo, hep-th/0411069.
- ⁵⁵A. Voros, *J. Phys. A* **32**, 1301 (1999); **32**, 5993 (1999); **33**, 5783 (2000).
- ⁵⁶L. N. Trefethen, A. E. Trefethen, S. C. Reddy, and T. A. Driscoll, *Science* **261**, 578 (1993); S. C. Reddy and L. N. Trefethen, *SIAM J. Appl. Math.* **54**, 1634 (1994); E. B. Davies, *Commun. Math. Phys.* **200**, 35 (1999); A. Aslanyan and E. B. Davies, *Numer. Math.* **85**, 525 (2000); M. Zworski, *Commun. Math. Phys.* **229**, 293 (2002).
- ⁵⁷U. Günther, P. Moniz, and A. Zhuk, *Phys. Rev. D* **68**, 044010 (2003); U. Günther, A. Zhuk, V. Bezerra, and C. Romero, hep-th/0409112.
- ⁵⁸A. Gailitis *et al.*, *Phys. Rev. Lett.* **84**, 4365 (2000); **86**, 3024 (2001); U. Müller and R. Stieglitz, *Phys. Fluids* **13**, 561 (2001); A. Gailitis *et al.*, *Rev. Mod. Phys.* **74**, 973 (2002).
- ⁵⁹K.-H. Rädler and H.-J. Bräuer, *Astron. Nachr.* **308**, 101 (1987).